AIAA 2001-0569

Evaluation of Computational Aeroelasticity Codes for Loads and Flutter

Larry Huttsell
Air Force Research Laboratory, WPAFB OH

Dave Schuster
NASA Langley Research Center, Hampton VA

John Volk
Northrop Grumman, El Segundo CA

Joe Giesing
The Boeing Company, Long Beach, CA

Mike Love
Lockheed Martin, Fort Worth, TX

39th Aerospace Sciences Meeting & Exhibit
January 8–11, 2001 / Reno, NV

AIAA-01-0569

EVALUATION OF COMPUTATIONAL AEROELASTICITY CODES FOR LOADS AND FLUTTER

Larry Huttsell*, Air Force Research Laboratory, WPAFB Ohio 45433
Dave Schuster+, NASA Langley Research Center, Hampton VA 23681
John Volk**, Northrop Grumman, El Segundo CA 90245
Joe Giesing++, The Boeing Company, Long Beach CA 90807
Mike Love*, Lockheed Martin, Fort Worth TX 76108

ABSTRACT

This paper presents an overview of a joint effort to evaluate computational aeroelasticity codes for loads and flutter. Computations are performed on realistic problems for static aeroelasticity, classic flutter, Limit Cycle Oscillations (LCO), and control surface buzz. The codes being evaluated involve a transonic small disturbance code with an interactive boundary layer method and two Euler/Navier-Stokes codes. To evaluate the accuracy of these codes, comparisons are made with available wind tunnel or flight test data. This paper presents the results/status of the following applications: static aeroelasticity – aeroelastic tailored wing, flutter – AV-8B-like wing and F-15-like tail, LCO – B-1-like and B-2, and control surface buzz – NASP wind tunnel model and Global Hawk wing.

NOMENCLATURE

α, AOA	=	Angle of Attack
CG	=	Center of Gravity
g	=	Damping
M	=	Mach Number
Q, q	=	Dynamic Pressure
Re	=	Reynolds Number

INTRODUCTION

Aeroelasticity is the study of the mutual interaction of the aerodynamic, elastic, and inertial forces on a structure. Static and dynamic effects can be accurately and inexpensively for subsonic and supersonic speeds, predicted using software that combines a linear finite element formulation for the structure with linear aerodynamic methods such as the doublet-lattice method. For the nonlinear transonic regime, most aircraft development programs require expensive flutter models and extensive wind tunnel and flight testing. With the current procedures, many of our recent aircraft have experienced problems due to inaccurate prediction of aerodynamic loads that involve nonlinear phenomena such as shocks, vortices, and separated flow. Examples include adverse static aeroelastic effects such as increased trim drag and loss of control effectiveness, transonic flutter, Limit Cycle Oscillations (LCO), and control surface buzz. With the advances in Computational Fluid Dynamics (CFD) and computer technology, Computational AeroElasticity (CAE) is an emerging technology with high potential for analysis and design of structurally flexible vehicles in flight regimes involving nonlinear aerodynamics. Several computational aeroelasticity methods have been undergoing development and research applications for a number of years[1-7].

Under the national Fixed Wing Vehicle Program, the major aerospace companies formed an Airframe Technology Advisory Group to identify elements of "precompetitive airframe technology" that could be pursued within a collaborative-shared investment. The area of Aerodynamics/Structures/Controls Interaction (ASCI) was identified for investigation. One of the specific efforts for collaboration was the evaluation of computational aeroelasticity codes on real-world problems. An AFRL contract to Boeing and Northrop Grumman with in-kind contributions from industry and in-house support from NASA Langley initiated this ASCI effort. Under internal funding, Lockheed Martin is also developing and testing a computational aeroelasticity method that loosely couples their CFD code SPLITFLOW[8] with established structural finite element methods. The analysis codes are integrated through the object-oriented Multi-Disciplinary

---

* Senior Aerospace Engineer, AIAA Associate Fellow
+ Senior Research Engineer, AIAA Associate Fellow
** IPT Lead, AIAA Senior Member
++ Boeing Technical Fellow, AIAA Associate Fellow
* Engineer Specialist Senior, AIAA Senior Member

Computing Environment (MDICE)[9] and the system is being used to predict aircraft flight loads[10]. This paper focuses on the contracted effort that evaluates government-developed and supported CAE methods.

In the first phase of this contracted ASCI effort, the industry partners determined the criteria for the code evaluation. In the second phase, the industry and the government teams selected the codes for evaluation and the application cases. In the third and current phase, the codes are being evaluated on five types of aeroelastic problems: static aeroelasticity, flutter, two types of Limit Cycle Oscillations (LCO), and control surface buzz. This paper will present preliminary results and the current status of the applications under this ASCI effort.

COMPUTATIONAL CODES

Three computational aeroelasticity methods have been chosen for evaluation under the ASCI program. Two of these methods employ high-level computational aerodynamics in the aeroelastic solution process while the third method takes a more computationally efficient, approximate approach to the simulation of the aerodynamics. The three methods use a similar structural dynamics model that reduces the structural problem to a set of mode shapes and frequencies. The simplest and most efficient of the methodologies chosen solves the transonic small disturbance equations and is known as CAP-TSD. The basic inviscid form of this method has been modified to include an inverse boundary layer coupling (CAP-TSDV) which has been shown to be very effective in predicting weakly separated and separation onset flows. The higher-level methods, known as ENS3DAE and CFL3D, solve the Reynolds-averaged Euler/Navier-stokes equations for compressible flow and are applicable to a wider range of flows than CAP-TSDV at the cost of significantly greater computational and manpower expense. All three codes provide the capability to perform time-accurate modeling of dynamic phenomenon.

CAP-TSD

CAP-TSD[1,11] solves the three-dimensional transonic small disturbance potential flow equations for partial and complete aircraft configurations. The standard, most widely distributed version of the program computes inviscid compressible flow for combinations of wings, fuselage, horizontal tail, bodies/stores, and rectangular planform vertical surfaces. CAP-TSD solves the aerodynamic equations of motion using a time-accurate algorithm[12] that is capable of simulating both steady and unsteady flow. The method is capable of computing aeroelastic simulations by coupling the aerodynamic module with a structural dynamics simulation. The structural dynamics of horizontal surfaces are simulated in CAP-TSD by using a modal structural model. The structural analysis is coupled to the aerodynamic analysis by a process that transfers generalized aerodynamic forces and generalized displacements between the aerodynamics and structural dynamics modules. Using this approach, CAP-TSD is capable of simulating both static and dynamic aeroelastic phenomena.

A viscous-inviscid interaction version of CAP-TSD, known as CAP-TSDV has been developed[13,14] and applied to a variety of problems involving mildly separated and separation onset flows[15,16]. The method couples the inviscid CAP-TSD algorithm with an inverse integral boundary layer model. The boundary layer equations are solved in a quasi-steady formulation similar to that recommended by Green, et al[17]. The outer inviscid solution and the inner viscous solution are computed independently and are coupled using an active control mechanism that minimizes coupling errors for unsteady flows.

CAP-TSD solves the equations of motion on a sheared Cartesian grid system where lifting surfaces are modeled as thin plates. Thickness and camber information for the upper and lower surfaces of each lifting surface is supplied through a set of surface slopes that are specified as boundary conditions for the code. Similarly, structural mode shapes are also supplied as surface slope perturbations. This approach greatly simplifies the modeling task required for an aeroelastic analysis since the grids are typically simple to generate, and no moving grid algorithm is required for the aeroelastic simulation. Thus CAP-TSD is a very efficient alternative to higher order methods which can be 1 - 1.5 orders of magnitude more computationally intensive than CAP-TSD. The CAP-TSDV version of the code is being used for these applications since the viscous capabilities are required for the phenomenon being modeled.

ENS3DAE

One Euler/Navier-Stokes aeroelastic analysis method chosen by the ASCI participants is known as the Euler/Navier-Stokes 3-Dimensional Aeroelastic (ENS3DAE) method. The Lockheed-Georgia

Company, under contract to the Air Force Wright Laboratory, developed ENS3DAE in the late 1980's[18]. This program has been used to solve numerous aerodynamic and aeroelastic problems about a wide range of geometries including wings, wing/fuselage, wing/control system, propulsion, and integrated airframe/propulsion configurations[19-21].

ENS3DAE solves the full three-dimensional compressible Reynolds averaged Navier-Stokes equations, the thin layer approximation to these equations or the Euler equations using an implicit approximate factorization algorithm. Central finite differences are used to spatially discretize the problem. A three-dimensional implementation of the Beam-Warming implicit scheme is employed for the temporal integration. Blended second and fourth order dissipation is added to the explicit right-hand-side of the equations, and implicit second order dissipation is added to improve the diagonal dominance of the matrix system. For time-accurate cases, a procedure that employs either global or local time stepping within an inner sub-iteration loop for each physical time step has been implemented. This procedure effectively removes the stability limit on the time-step for unsteady flow cases, but accuracy can suffer for large time-step cases when an insufficient number of sub-iterations are performed to converge the solution within a physical time-step.

The method accepts either single or multiple block curvilinear grids. Boundary conditions are imposed explicitly on each computational face of each grid block and the current release of the program requires a one-to-one match of grid points at block interfaces. Turbulence characteristics are predicted using the Baldwin-Lomax[22] algebraic turbulence model or the Johnson-King model[23]. The code has been explicitly written to take advantage of vectorization and directives for parallel operation on shared memory processors are also included in the programming. The method is regularly run on eight or more processors.

A linear generalized mode shape structural model is closely coupled with the aerodynamic method to analyze structurally flexible vehicles. Modal motion is also used for prescribed control surface motion. ENS3DAE uses a highly efficient grid motion algorithm for aeroelastic and control surface simulations that is based on an algebraic shearing technique. Since dynamic aeroelastic and oscillating control surface simulations require grid models that deform in time, a Geometric Conservation Law (GCL)[24] has also been incorporated in the code.

CFL3DAE

This ASCI effort is also evaluating aeroelastic versions of the NASA Langley developed Euler/Navier-Stokes code known as CFL3D[25]. The aerodynamic base version of the code has become a staple for computational aerodynamics research throughout the industry, but the aeroelastic versions of the code, (often referred to as CFL3DAE), have had limited application over the past 10 years.[4,26-28]

CFL3D solves the thin-layer three-dimensional compressible Reynolds averaged Navier-Stokes equations. The integral form of the equations is spatially discretized with volume integrals evaluated at cell centers and fluxes evaluated at cell faces. Typically, upwind differencing of the fluxes is used with third order upwind-biased Roe's flux difference splitting and a minmod flux limiter. Temporal simulations are usually accomplished using second order accurate backward time differencing. An implicit approximate factorization algorithm is used to solve the equations. Pseudo time sub-iteration coupled with an efficient multigrid algorithm is used to accelerate convergence at each time step. The code also includes a variety of turbulence models including the Spalart-Allmaras model[29] that has become increasingly popular among researchers due to its performance in the presence of separated flow and its robust character.

There have been several aeroelastic versions of the code developed and two of them were used to produce results in this paper i.e. version 4.1 and 6.0. The latest version[30] (6.0) incorporates a new deforming mesh scheme based on the spring analogy and incorporates the GCL in the Navier-Stokes equations as opposed to solving the GCL as a separate set of equations. The new grid deformation scheme pays particular attention to the treatment of the grid near wall boundaries and in the wake regions behind aerodynamic surfaces. Using the current approach, grid orthogonality near aerodynamic surfaces is maintained and the trailing wakes tend to smoothly leave surface trailing edges, even when aeroelastic and/or control surface deflections become large. A linear, normal mode structural dynamics model is closely coupled with the solution of the aerodynamic equations of motion to simulate aeroelastic problems. The structural dynamics equations of motion are solved using a predictor-corrector linear finite dimensional state space formulation of the uncoupled modal equations.

While ENS3DAE and CFL3DAE solve a very similar set of physical equations of motion, there are

significant algorithmic differences that might influence the simulation of unsteady aeroelastic problems. Primary among these is the central finite difference formulation of ENS3DAE versus the upwind finite volume formulation of CFL3DAE. It can certainly be argued that CFL3DAE represents a more modern approach to CFD analysis, but it should also be noted that the development of today's upwind schemes have been primarily optimized for steady flow simulations. This development process has tuned the algorithms to damp out a wide range of frequencies so as to more rapidly achieve a steady-state solution. Unsteady aeroelastic problems require that the numerical algorithms used to solve the equations of motion possess only small amounts of numerical damping, particularly at lower frequencies. Thus it is beneficial to maintain both of the chosen Euler/Navier-Stokes methods to assist in evaluating the role of numerical algorithm in the simulation of unsteady aerodynamic and aeroelastic problems.

RESULTS

To provide a realistic evaluation of these codes, configurations were selected that covered the five types of targeted aeroelastic problems. The configurations had to exhibit nonlinear aeroelastic behavior, have the necessary engineering data available to build the high fidelity aeroelastic models, and have available test data necessary for correlation. This section presents the current results or status of the on-going evaluation phase.

Static Aeroelastic Applications

Validation of Aeroelastic Tailoring Model

In the late 1970s, a validation of aeroelastic tailoring (VAT) study[31] was conducted by design, fabrication, and testing of static aeroelastic and flutter wind tunnel models. This study generated a wealth of data ideal for verification and validation of computational aeroelasticity methods. Included in the program were two opposite tailoring concepts: a washout concept and a washin concept. For the washout concept, composite layers were oriented such that the aeroelastic twist of the airfoil cross-sections *decreases* as the wing deflects up. For the washin concept, composite layers were oriented such that the aeroelastic twist of the airfoil cross-sections *increases* as the wing deflects up. Data was collected at transonic flight conditions for $1/9^{th}$ scale static aeroelastic models as well as a baseline rigid model. The data includes chordwise pressure distributions, static aeroelastic deflections measured through stereo photogrammetry, and total body forces and moments.

The ENS3DAE code was used to analyze the washout wing at M=0.9 and 9 degrees angle of attack. The grid used was a 2-block H-H grid (108x35x32) with clustering near the surface. The Baldwin Lomax turbulence model was used to predict the turbulence characteristics. The structure was represented by a set of influence coefficients (4 chordwise and 7 spanwise locations). The flexible wing (Figure 1) analysis compares very well with the experimental data over most of the span. The correlation on the upper surface near the tip is not as good as the inboard stations. Near the tip, the experimental data indicates a massive upper surface flow separation that is not captured by the analysis. The experimental data indicates a front spar deflection of 3 inches at the wing tip and ENS3DAE predicts a deflection of 2.8 inches at this station. A comparison of the computed and experimental wing twist distributions shows excellent agreement (wing twist within 0.1 degrees over virtually the entire wing).

Flutter Applications

F-15 Flutter Model

During the wind tunnel test of an F-15-like flutter model it was discovered that a snag in the leading edge near the root would favorably impact the flutter speed. This effect was not predicted using linear methods and so a correlation using CFL3DAE (V-4.1) is being attempted to see if a significant difference between flutter speed, with and without snag, can be predicted. Figure 2 depicts the model used, the mesh employed, and an initial steady/rigid solution for pressure coefficient. Four million grid points were used to determine the flow at a Mach number of 0.76 and angle-of-attack of zero degrees. It required over 35,000 iterations to converge. Unsteady flows have not yet been successfully completed due to negative volume problems being encountered with the grid perturbation routine. These problems occur mostly at the stabilizer tip probably due to the extreme warp of the O-grid in that region.

AV-8B Wind Tunnel Model

An attempt to correlate flutter speed that is a function of angle-of-attack is underway with CFL3DAE (V-4.1). Specifically a correlation of an AV-8B-like

clean-wing flutter observed on a wind tunnel model that displayed this nonlinear effect is being performed. An initial grid for the clean wing is shown in Figure 3. This grid has 3 million grid points contained in 29 blocks. Initial attempts to run this case have not been successful even for the steady rigid case. This case was analyzed using another steady Euler/Navier-Stokes analysis code, but the aerodynamic coefficients did not converge to a steady state and instead showed an oscillatory behavior. The steady analysis also indicates large areas of trailing edge separation. If the steady results are indicating a buffeting condition, it will be a very challenging test case for CFL3DAE or any other time-accurate code.

Limit Cycle Oscillation (LCO) Applications

B-2

The B-2 aircraft encountered a nonlinear aeroelastic Residual Pitch Oscillation (RPO) during low altitude high speed flight-testing.[32,33] The RPO response was observed after control surface pitch doublets were input at flight conditions outside the operational envelope. The initial air vehicle response decayed in amplitude but transitioned to a small, constant amplitude, residual pitch oscillation after several cycles as shown in Figure 4.

Analytical analysis and wind tunnel testing did not predict the RPO phenomenon before it was discovered in flight tests. Analytical aeroelastic models used linear aerodynamic representations, which were incapable of capturing the highly nonlinear nature of the RPO. A detailed description of the analytical and flight test program investigating this phenomenon is presented in References 15, 31, and 32. An important element of the RPO investigation was the application of CAP-TSDV to the simulation of this nonlinear aeroservoelastic event. Even though an operational solution has been implemented to help the pilots avoid encountering RPO, a high interest still remains in refining analysis predictions capabilities such that sensitivies to RPO can be analytically determined and investigated for future vehicles of this type. These ongoing analyses are summarized here.

Aerodynamic, structural and control system models were configured for the three codes under evaluation. All models were for a symmetric analysis about the vehicle centerline. The aerodynamic models were developed from a B-2 geometry definition referred to as the "nacelle subtracted moldlines" where the aircraft geometry has been modified in the area of the nacelle so that the inlet mass flow is approximately represented. Structural modes used in the aeroelastic analysis were obtained from a ground vibration test correlated structural finite element model. A control system model was configured to allow trim, as well as open and closed loop responses for time marching simulations. Two weight configurations are being studied - a heavy outboard fuel condition with forward c.g. and a light outboard fuel condition with forward c.g. The heavy condition was found to be the most critical, with near zero damping seen in flight test. The light condition showed an interesting trend in flight test whereas the damping approached zero, then returned to a stable system with increasing Mach, commonly referred to as a "hump mode".

A sheared-Cartesian grid suitable for computations using CAP-TSDV was developed. The grid consists of 300,000 grid points, 100 streamwise, 60 spanwise, and 50 vertical with 60 of the streamwise and 40 of the spanwise points residing on the B-2 planform. An illustration of the wing planform as modeled for CAP-TSDV is compared with that of the actual vehicle in Figure 5. The B-2 aircraft wing tip and control surfaces edges are planform aligned and are not streamwise as on typical aircraft. Therefore the CAP-TSDV modeling of the wing required several approximations. Since tightly packed grid lines are can cause poor convergence in CAP-TSD, a clipped wing tip was defined. The wing tip model possesses the same planform area as the actual wing planform. The flight control surfaces were modeled by selecting constant chord and streamwise grid lines, which best approximated the actual geometry. The middle elevon was not modeled since it does not actively move during the RPO responses.

The chordwise static pressures computed by CAP-TSDV are compared with wind tunnel data measured on a 6% scale model in Figure 6. These plots show upper, lower, and delta coefficients of pressure (Cp) at spanwise station 474, which corresponds to the middle of the inboard elevon, for the heavy configuration at 4,000 altitude and Mach 0.8. Results for conditions of approximately zero angle-of-attack are shown. Note Cp upper and Cp lower are plotted on left and right vertical axes respectively. The Cp lower results are plotted unconventionally, with negative values down, for clarity. The upper/lower differential Cp results show good agreement with the wind tunnel data.

Dynamic simulations were started from saved static aeroelastic trim solutions and run for a sufficient time to evaluate the stability characteristics of the vehicle.

Inboard elevon control surface doublet commands were used to perturb the air vehicle. Simulations for both open and closed loop control laws were generated, and dynamic aeroelastic simulations were run at a series of Mach numbers to determine the stability characteristics. Transient responses of the vehicle angle-of-attack were used to extract damping and frequency information. Large amplitude pitch doublet excitations were used and the damping properties were extracted in the first 3 seconds of the response, prior to the onset of constant amplitude residual pitch oscillations.

Dynamic aeroelastic simulations were run for a heavy configuration at 4,000 feet altitude for a series of Mach numbers with 1-degree inboard elevon doublet excitations. Angle-of-attack transient responses for several open and closed loop control law simulations at several Mach numbers are shown in Figure 7. The CAP-TSDV open and closed loop 4,000 foot altitude stability boundary for the heavy configuration is compared to flight test results in Figure 8. The flight test results are shown with symbols, for the raw data, and a fitted curve. The damping curve fit used the minimum damping values at each Mach number. The flight control system closed versus open loop simulation results tend to slightly increase the frequency of the RPO motion and raise the Mach number of the neutrally stable point. The CAP-TSDV frequencies are slightly lower than the flight results. The damping for the closed loop CAP-TSDV simulations compare well with flight test. The abrupt slope change at 0.785 Mach number is believed to be associated with the development of shocks as shown in Figure 9. This plot shows station 345 closed loop upper and lower surface pressure coefficients (Cpu and Cpl) for several Mach numbers. Station 345 is located outboard of the engine nacelles and passes through the inboard elevon. Shocks begin to develop around Mach 0.785 and become very strong by Mach 0.835. The significant change in the pressure distributions cause large movements in the aircraft aerodynamic center and verifies hypotheses formed from analysis of the flight test data.

Dynamic aeroelastic simulations were also run for a light configuration at 4,000 feet altitude. Extracting the frequency and damping data for the light configuration was more difficult than the heavy configuration due to the highly damped character of the response at the lower Mach numbers. The lighter weight short period damping was generally much higher than typical structural modes. Higher quality frequency and damping data could be computed in CAP-TSDV in the future by making enhancements that would allow control surface frequency sweeps or random excitation inputs.

The light configuration open and closed loop 4,000 foot altitude stability boundary is compared to flight test results in Figure 10. The CAP-TSDV closed loop frequencies appear to abruptly change near Mach 0.8 where there is a shift in the dynamic character of the aircraft from short period pitch dominated motion to one that is highly influenced by the first wing bending mode. CAP-TSDV simulation and flight results have similar damping up to Mach 0.82, where the flight results exhibit a hump mode character. The hump mode character did not appear during the simulations. The cause of this difference has not been determined and is a subject of future studies. Two hypotheses for the source of the difference are: 1) the degree of flow separation is under predicted and in flight the flow separation helps quench the oscillations, and 2) the spanwise flow in separated regions, disrupts the shock development. Both of these characteristics represent phenomena that are likely beyond the transonic small disturbance capabilities of CAP-TSDV and warrant further investigation using higher order methods.

A Navier-Stokes aerodynamic model was configured from the same B-2 geometric moldlines as the CAP-TSDV model. The grid is a 109x169x81 C-H grid giving 1.5M grids. The wing tip was clipped, but only slightly, and offered an improved representation of the configuration over the CAP-TSDV model. Similar to the CAP-TSDV grid, the streamwise and chordwise point distributions were tailored to approximate the gust load alleviation system and inboard and outboard elevons. Figure 11 illustrates the CFL3DAE (V-6.0) CFD grid. CFL3DAE (V-6.0) results are compared to both wind tunnel and CAP-TSDV results in Figure 12. Chordwise cuts of the pressure coefficient distribution at wing stations 321 and 474 are illustrated for a condition approaching the RPO onset point for the heavy configuration. All correlations are quite good, with the CFL3DAE (V-6.0) computations showing an improvement over CAP-TSDV. Figure 13 illustrates isosurfaces illustrating the Mach 1.0 boundary, which gives a clear graphical representation of the strong shock formations on both the upper and lower surfaces. Dynamic aeroelastic simulations with CFL3DAE and ENS3DAE are pending code updates that allow for vehicle trim and rigid body mode inclusion, replicating what was done in CAP-TSDV.

B-1

The CFL3DAE (V-4.1) Navier-Stokes code was correlated with wind tunnel results that displayed a LCO phenomenon on a B-1-like configuration[34]. This LCO was characterized by a coupling of aerodynamic forces due to vortical flow with the elastic response of a wing structure. The geometric and the structural modeling were taken from the B-1 aircraft with the nacelle removed to reduce complexity while still maintaining the basic LCO mechanisms. The first four structural modes were used. This cutoff was chosen as a trade-off between numerical efficiency and fidelity of the structural representation for the dynamic aeroelastic solutions. The flow conditions were specified to match the wind tunnel data.

Initially the steady rigid and static aeroelastic solutions were computed to furnish a converged starting point for the dynamic solutions and to gain an understanding of the flow phenomenon that prompts the LCO. Figures 14 and 15 present computed flow-field results for these two steady conditions. The vortex patterns are very complicated and the wing tip is stalled.

From the experiment it is known that the LCO phenomenon is very sensitive to angle-of-attack, i.e. it was observed only within an angle-of-attack range of less than half a degree. To effectively capture the LCO, time accurate solutions were computed for unsteady, transonic (M_∞=0.975), and viscous (Re_c=5.9 million) flows over this B-1-like wing-body configuration at angles-of-attack of 7.38, 7.88, 8.00, 8.13, 8.25, and 8.38 degrees. Phase diagrams and aerodynamic damping estimates are used to identify LCO damping. Figure 16 presents the predicted LCO damping that appears to capture the trends of the experimental data even with the simplifying assumptions used. The wing tip deflections during LCO were however considerably smaller than the observed wind tunnel or associated flight-test results.

Figure 17 presents computed instantaneous streamlines during LCO motions. These streamlines correlate well with experimental oil flow images (not shown). Finally, the choice of the computational time step size is identified as a major factor in modeling the development of LCO. Information on the streamlines, time steps, and other details can be found in Reference 33. Correlation with the ENS3DAE code is also planned.

Buzz Applications

Global Hawk

The Northrop Grumman Global Hawk, shown in Figure 18, is an Unmanned Reconnaissance aircraft capable of long endurance, high altitude flight. The high aspect ratio wings have midspan inboard and outboard ailerons. During high altitude flight tests in turbulent conditions several instances of aileron buzz were recorded. These events were the result of turbulence-induced overspeeds, outside of the flight envelope. The phenomenon manifests itself as an uncommanded, high frequency, limited amplitude oscillation of the ailerons which occurs abruptly above a specific high speed point, and similarly stabilizes when the airspeed is brought below the threshold. Flight test data was examined to characterize the phenomenon. The aircraft was well instrumented with typical air data and flight parameters being recorded in conjunction with loads on both the right hand and left hand inboard and outboard aileron. Results showed that the phenomenon was clearly Mach dominated, with an abrupt onset of the buzz on all four ailerons at a distinct Mach threshold. The outboard ailerons undergo a more pronounced response then the inboard. This is essentially consistent with design guidelines indicating that a more outboard, lower chord surface would be more prone to buzz. The right and left inboard aileron response indicates a symmetric response. Due to the high aspect ratio nature of the vehicle and placement of the ailerons, it is felt that the problem can be well represented symmetrically, as virtually no aerodynamic and minimal structural interaction would be expected between the right and left aileron sets.

Figure 19 is a Fourier Transformation of the time history of the right inboard aileron during a buzz event. The frequency of oscillation is 23 Hz., somewhat lower than the free vibration frequency of 28 Hz. No other significant frequency content is noted. This is consistent with what might be expected from classical buzz, which is predominantly a single degree of freedom aeroelastic phenomenon of a control surface rotational mode. The frequency shift down may be due to a small freeplay in the control system. What is unknown is the specific aerodynamic phenomenon that triggers the phenomenon - hopefully to be indicated by the codes being studied.

The Global Hawk loft lines where obtained for aerodynamic modeling purposes. A CAP-TSDV aerodynamic model has been configured and is in the debugging mode. The model is a wing only model -

with the wing root fairing extended to the centerline. Since the vehicle has a very large wingspan, a slender fuselage, and the aileron is placed on the outboard section of the wing, the vehicle can be confidently modeled as a semispan wing-alone configuration. The CAP-TSDV model consists of 80 points in the streamwise direction, 56 points spanwise and 60 points normal for a total of 270,000 grid points. The wing surface is comprised of a 40x40 mesh, with breaks consistent with the aileron chordwise and spanwise breaks. The boundary layer model begins at approximately the 18% chord extending to the trailing edge. Debugging of the aerodynamic model is in process.

A symmetric 93x225x81 C-H mesh was created for the CFL3DAE and ENS3DAE Navier-Stokes codes as displayed in Figure 20. Figure 21 illustrates a cross sectional cut at mid aileron for a rigid CFL3DAE run within the known buzz regime. It is evident that a strong shock has set up on the upper surface, with separated flow from approximately the 40% chord onward, with the lower surface flow remaining attached. Total force data compared well with available computational and test data. Figure 22 illustrates that the pressure profiles show minimal change over the span - which is to be expected for a high aspect ratio wing, slender fuselage configuration.

The NASTRAN Finite Element structural model developed for flutter analysis was used to compute the structural modes (9 selected) for the CAP-TSDV, CFL3DAE and ENS3DAE aeroelastic analysis. The structural modes were augmented to approximate the control surface free-play, and the modes were interpolated to the aerodynamic surfaces.

Control surface buzz is often associated with control surface free-play, which is always present to some degree. Free-play presents a non-linear structural behavior, whereas the aileron rotational stiffness is very low throughout the free play range, but jumps to a nominal high stiffness value at and above the freeplay boundary. The nominal value is determined by the actuator stiffness, control surface mass, and the stiffness of the backup structure. As none of the three codes have a non-linear structural capability, an approximation was made for the aeroelastic simulations. For purposes of the simulation the nominal structural stiffness of the aileron mode was reduced by a factor of 100, which reduces the free vibration frequency to 1/10th nominal. It is anticipated that this approximation will result in the simulations showing the onset of the buzz phenomenon. However, the amplitude of the oscillations would not be expected to be realistic as the high stiffness regime is eliminated. This is another case where real world problems demonstrate the need of future tool enhancement - in this case a non-linear structural modeling capability. Aeroelastic solutions are in process for the three codes being evaluated, with results to be reported at a future date.

Generic NASP Wing with Control Surface

Correlation of the CFL3DAE (V-4.1) Navier-Stokes and CAP-TSDV transonic small disturbance codes with transonic wind tunnel results were undertaken for a National Aerospace Plane (NASP) hypersonic wing model with a control surface. The model[35] was tested in the NASA Langley Transonic Dynamics Tunnel and is described in Figure 23. It consisted of a 60-degree delta wing made up of a stiff steel plate covered with balsa wood to provide a 3% thick symmetric circular arc wing section. The model also had a full span control surface constrained with an elastic spring.

Figure 23 also shows the size for the H-H two-block grid for CFL3DAE (V-4.1), the Mach numbers considered, and the number of steady and unsteady computations undertaken. Figure 24 presents the correlation of CFL3DAE with the test data for 7 of the 13 cases computed that were closest to the buzz boundary. An approximate buzz boundary was estimated from these cases. In some instances it was difficult to determine whether the motion was stable or unstable e.g. $M = 0.96$, $q = 90$ psi. In most cases it required many cycles to accurately determine the stability of the flow condition. A particularly difficult case is shown at $M = 0.98$, $q = 90$ psi where the nonlinear motion imitates the beating of closely spaced modes even though it is a single degree of freedom phenomenon. The approximated buzz boundary compares favorably with the test results. It is clear that CFL3DAE (V-4.1) would be a very beneficial tool to indicate if buzz will occur and approximately where it will occur. The predicted frequencies, also shown in Figure 24, compare well with the test results indicating that the proper buzz mechanism has been captured.

Some apparent but small flow anomalies were observed in the steady flow solutions. Specifically, Figure 25 shows a snapshot in time of a steady flow condition that produced a slight time-dependent flow near the trailing edge. Trailing edge separation is alternately growing and decreasing in time on the upper and lower surfaces, but does not appear to be shedding.

It is questionable whether this is a physical or numerical phenomenon. Figure 26 illustrates the shock motion for a control surface flapping. Notice that the shock passes over the hinge line for a peak-to-peak control surface amplitude of less than 3 degrees. The cross-sectional view is for a section cut at the centerline of the wing. Generally speaking CFL3DAE (V-4.1) provided good qualitative results for predicting a difficult flow phenomenon. All of the flow conditions converged to acceptable residuals. Some flow phenomenon such as the separation at the trailing edge may be questionable as to their physical existence.

Figure 27 shows the size for the H-H single-block grid for CAP-TSDV, the Mach numbers considered, and the number of steady and unsteady computations undertaken. Figure 28 presents the correlation of CAP-TSDV with the test data for 11 of the 13 cases computed. Several M = 1.0 cases did not converge for either steady or unsteady calculations. At M = 0.98 the steady flow converged but the unsteady flow did not as shown in Figure 29. For the two cases at M = 0.97 the flow converged but the resulting solutions were not physically understandable. Further analyses using CAP-TSDV are required to determine the sources of these problems.

An approximate buzz boundary was estimated from the cases run and is shown in Figure 28. This boundary does not compare extremely well with the test results, however it is clear that CAP-TSDV could be used to indicate if buzz would occur and roughly where it will occur. The predicted frequencies, also in the figure, are qualitatively similar to the test results indicating that the proper buzz phenomenon has been captured. It was easier to distinguish the stability of CAP-TSDV cases compared to the CFL3DAE cases due to the nonlinear behavior of the latter, however it is concluded that CFL3DAE (V-4.1) is clearly of higher fidelity and produces a better comparison with test data.

CONCLUSIONS

Three computational aeroelasticity codes are being applied to complex configurations where nonlinear aerodynamics are present. The test cases chosen present a number of challenges to the CAE methods ranging from modeling of complex geometries to prediction of highly nonlinear complex flowfields and structural interactions. The test cases have provided invaluable insight into the capabilities and shortcomings of the various methods employed, and have directed developers to areas where improvements can be realized. As suspected from the outset of this exercise, there is no clear method-of-choice which comes from these analyses, and the ASCI program was never intended to be a competition among the codes. The methods employed in these analyses are research tools that require further improvements and validation before enjoying a production status. In many cases, these codes have been placed in the hands of users who are not intimate with their operation or development. This approach has quickly and efficiently identified the shortcomings of the various methodologies and provided an excellent guide for future CAE development. The individual selected applications have also been very useful in this regard with each application identifying at least one area where improvements in the available methodology could better equip the given method for future applications.

Many of the applications have clearly shown that simply coupling fluid and structural interactions is not sufficient to model, predict and correct many of the problems encountered on modern air vehicles. For instance, the RPO phenomenon encountered on the B-2 Bomber was quickly shown to be a complex interaction between the nonlinear aerodynamics and the flexible structure of the vehicle, and its short period rigid body mode. Developers of the CAP-TSDV code have shown that a trimmed, free-flying vehicle with open and closed loop flight control systems can be readily modeled in CAE analyses. This demonstration has further inspired developers of higher order methods to add these capabilities to their codes, and the CFL3DAE (V-6.0) and ENS3DAE codes are being modified to include this capability.

The ability to model structural nonlinearities has also been shown to be an important factor in some of the problems analyzed. The Global Hawk and the hypersonic wing buzz computations would both significantly benefit from a control surface freeplay model in the aeroelastic analysis.

Finally, the ability to accurately and efficiently predict separated flow and model geometrically complex configurations was further underscored by the AV-8B wing analysis and the F-15 empennage simulation. The flutter computations on the AV-8B and the F-15 empennage both demonstrate the continued emphasis on grid generation and grid motion strategy development for dynamic aeroelastic analyses. Geometry modeling technology along with the development of accurate and efficient unsteady aerodynamic algorithms continue to be the primary

pacing items for the development of high-order CAE tools.

A few specific characteristics pertaining to the individual codes have been observed. The modeling and computational efficiency of CAP-TSD makes it a natural initial selection for any project faced with the simulation of a dynamic aeroelastic problem. For experienced users, CAP-TSD can be used to quickly and effectively investigate a wide range of aeroelastic phenomena, and only after it has clearly been demonstrated that the methodology is unsuitable for the analysis task at hand should higher-order methodologies be considered. Once the commitment to implement higher order methods has been accepted, the choice of methods becomes more a matter of user-familiarity than the computational efficiency of the algorithms. The modeling challenges associated with the Euler/Navier-Stokes methodologies can easily grind any analysis program to a halt if the user is not familiar and comfortable with the tools and techniques required to build and implement suitable models. In general, CFL3DAE seems to be more robust than ENS3DAE for a variety of grids, and the algorithm and turbulence modeling selections associated with this method are more current than for ENS3DAE. However, there is virtually no evidence that shows that, given a properly formulated and developed grid model, ENS3DAE would generate an inferior result to that of CFL3DAE. Thus the choice of method continues to be primarily one of user preference.

This effort has provided a learning experience for the engineers involved, provided guidance for future code development, and identified areas for improvements. The Euler/Navier-Stokes codes show significant potential for static flight loads computations, but they are still very computationally expensive for dynamic cases. This effort has also demonstrated the value of using realistic and complex configurations for code evaluation. Improvements have been made to the codes as a result of these applications that will benefit future applications and valuable data has been generated for future code validation and verification. The final applications and evaluation of these codes will be completed and presented in future publications. Additional work is planned with MDICE[9] for static aeroelastic analysis of the Active Aeroelastic Wing Configuration. A new FY02 effort is planned to add a control system module to MDICE and validate it with the B-2 RPO data. Another area that needs to be address is the assessment of accuracy of load transfer and displacement across multiple domains (e.g. flap to flap, structural box to box, etc).

ACKNOWLEDGMENTS

The authors want to acknowledge John Edwards for his support of CAP-TSDV and Bob Bartels for his support of CFL3DAE. The authors would also to like to acknowledge the following engineers who contributed to this effort: Peter Hartwich, Chan-gi Pak, Geojoe Kuruvila, Myles Baker, Dave Dreim, and Dave Solomon. This work was supported in part with computer resources from the DoD Major Shared Resource Center at ARL.

REFERENCES

[1] Batina, J. T., "Unsteady Transonic Algorithm Improvements for Realistic Aircraft Applications," *Journal of Aircraft*, Volume 26, February 1989, pp. 131-139.

[2] Schuster, D. M., J. Vadyak, and E. Atta, "Static Aeroelastic Analysis of Fighter Aircraft Using a Three-Dimensional Navier-Stokes Algorithm," *Journal of Aircraft*, Volume 27, Number 9, September 1990, pp. 820-825.

[3] Guruswamy, G. P. and Byun, C., "Fluid-Structural Interactions Using Navier-Stokes Flow Equations Coupled with Shell Finite Element Structures", AIAA Fluid Dynamics Conference, AIAA Paper 93-3087, July 6-9, 1993.

[4] Lee-Rausch, E. M. and Batina, J. T., "Wing Flutter Computations Using an Aerodynamic Model Based on the Navier-Stoles Equations," *Journal of Aircraft*, Volume 33, Number 6, November-December 1996, pp. 1139-1147.

[5] Alonso, J., Martinelli, L., and Jameson, A., "Multi-grid Unsteady Navier-Stokes Calculations with Aeroelastic Applications", AIAA Paper 95-0048, 33rd Aerospace Sciences Meeting, Reno NV, January 1995.

[6] Farhat, Charbel, "High Performance Simulation of Coupled Nonlinear Transient Aeroelastic Problems", *Parallel Computing in CFD*, AGARD-R-807, October 1995.

[7] Melville, R., "Nonlinear Simulation of F-16 Aeroelastic Instability", AIAA Paper 2001-0570, January 2001.

[8] Karman, S. L. Jr., "SPLITFLOW: 3D Unstructured Cartesian/Prismatic Grid CFD Code for Complex Geometries", AIAA Paper 95-0343, April 1995.

[9] Siegel, J. M., Jr., et al., "Application of a Multi-Disciplinary Computing Environment (MDICE) for Loosely Coupled Fluid-Structural Analysis", Presented at the 7th AIAA/USAF/NASA/ISSMO Symposium of MDO, AIAA Paper 98-4866, September 1998.

[10] Love, M., De La Garza, A., Charlton E., and Egle, D., "Computational Aeroelasticity in High Performance Aircraft Flight Loads", ICAS 2000 Congress, 27 Aug – 1 Sept 2000.

[11] Batina, J. T., "Efficient Algorithm for Solution of the Unsteady Transonic Small-Disturbance Equation," *Journal of Aircraft*, Volume 25, July 1988, pp. 598-605.

[12] Batina, J. T., "A Finite Difference Approximate-Factorization Algorithm for Solution of the Unsteady Transonic Small-Disturbance Equation," NASA TP 3129, January 1992.

[13] Howlett, J. T., "Efficient Self-Consistent Viscous Inviscid Solution for Unsteady Transonic Flow," *Journal of Aircraft*, Vol. 24, November 1987, pp. 737-744.

[14] Edwards, J. W., "Transonic Shock Oscillations Calculated with a New Interactive Boundary Layer Coupling Method," AIAA Paper 93-0777, January 1993.

[15] Edwards, J. W., "Calculated Viscous and Scale Effects on Transonic Aeroelasticity," AGARD-R-822, Numerical Unsteady Aerodynamic and Aeroelastic Simulation, March 1998, pp. 1-1 - 1-11.

[16] Dreim, D. R., Jacobson, S. B., and Britt, R. T., "Simulation of Non-Linear Transonic Aeroelastic Behavior on the B-2," NASA CP-1999-209136, CEAS/AIAA/ICASE/NASA Langley International Forum on Aeroelasticity and Structural Dynamics 1999, June 1999, pp. 511-521.

[17] Green, J. E., Weeks, D. J., and Brooman, J. W. F., "Prediction of Turbulent Boundary Layers and Wakes in Compressible Flow by a Lag-Entrainment Method," R & M No. 3791, British Aeronautical Research Council, 1977.

[18] Schuster, D. M., Vadyak, J., and Atta, E., "Flight Loads Prediction Methods for Fighter Aircraft", WRDC-TR-89-3104, November 1989.

[19] Smith, M. J., Schuster, D. M., Huttsell, L. J., and Buxton, B., "Development of and Euler/Navier-Stokes Aeroelastic Method for Three-Dimensional Vehicles with Multiple Flexible Surfaces," AIAA Paper 96-1400, April 1996.

[20] Schuster, D. M., Beran, P. S., and Huttsell, L. J., "Application of the ENS3DAE Euler/Navier-Stokes Aeroelastic Method," AGARD-R-822, Numerical Unsteady Aerodynamic and Aeroelastic Simulation, March 1998, pp. 3-1 - 3-11.

[21] Lewis, A. P. and Smith, M. J., "Euler-Based Aeroelastic Analysis of Shell Structures," *Journal of Aircraft*, Vol. 37, No. 5, September-October 2000, pp. 840 - 845.

[22] Baldwin, B. and Lomax, H., "Thin Layer Approximation and Algebraic Model for Separated Turbulent Flow", AIAA Paper 78-257, 1978.

[23] Johnson, D. A., and King, L. S., "A new Turbulence Closure Model for Attached and Separated Turbulent Boundary Layers, AIAA Journal, Vol. 23, No.11, November 1985.

[24] Thomas, P. D., and Lombard, C. K., "Geometric Conservation Law and Its Application to Flow Computations on Moving Grids," *AIAA Journal*, Volume 17, Number 10, October 1979, pp. 1030 - 1037.

[25] Krist, S. L., Biedron, R. T., and Rumsey, C. L., "CFL3D User's Manual (Version 5.0)", NASA/TM-1998-208444, June 1998.

[26] Lee-Rausch, E. M. and Batina, J. T., "Wing Flutter Boundary Prediction Using Unsteady Euler Aerodynamic Method," *Journal of Aircraft*, Volume 32, Number 1, March-April 1995, pp. 416-422.

[27] Bartels, R. E. and Schuster, D. M., "A Comparison of Two Navier-Stokes Aeroelastic Methods Using BACT Benchmark Experimental Data," *Journal of Guidance, Control, and Dynamics*, Volume 23, Number 5, November-December 2000, pp. 1094-1099.

[28] Baker, M. L., Mendoza, R., and Hartwich, P. M., "Transonic Aeroelastic Analysis of a High Speed

Transport Wind Tunnel Model," AIAA Paper 99-1217, April 1999.

[29] Spalart, P. and Almaras, S., "A One-Equation Turbulence Model for Aerodynamic Flows," AIAA Paper 92-0439, 1992.

[30] Bartels, R. E., "An Elasticity Based Mesh Scheme Applied to the Computation of Unsteady Three Dimensional Spoiler and Aeroelastic Problems," Paper 99-3301, 14th AIAA Computational Fluid Dynamics Conference, Norfolk VA, June 28-July 1, 1999.

[31] Rogers, W. A., et al., "*Validation of Aeroelastic Ttailoring by Static Aeroelastic and Flutter Tests*", AFWAL-TR-81-3160, September 1982.

[32] Jacobson, S. B., Britt, R. T., Dreim, D. R., and Kelly, P. D., "Residual Pitch Oscillation (RPO) Flight Test and Analysis on the B-2 Bomber", AIAA Paper 98-1805, 39th SDM Conference, Long Beach CA, April 1998.

[33] Britt, R. T., Volk, J. A., Dreim, D. R., Applewhite, K.A., "Aeroservoelastic Characteristics of the B-2 Bomber and Implications for Future Large Aircraft", RTO Meeting in Ottawa, February 2000.

[34] Hartwich, P., Dobbs, S., Arslan, A., and Kim, S., "Navier-Stokes Computations of Limit Cycle Oscillations for a B-1-Like Configuration", AIAA Paper 2000-2338, AIAA Fluids 2000, Denver CO, June 2000.

[35] Parker, E. C., Spain, C. V., and Soistmann, D. L., "Aileron Buzz Investigated on Several Generic NASP Wing Configurations", AIAA Paper 91-0936, April 1991.

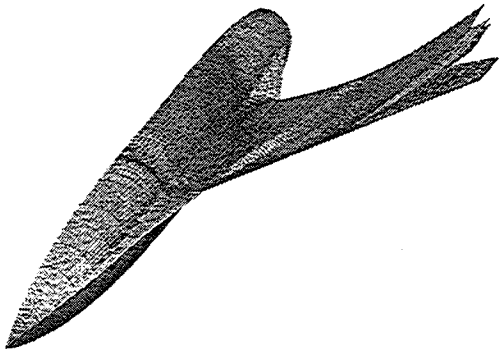

Figure 1. Static Aeroelastic Deflections for Aeroelastically Tailored Wing

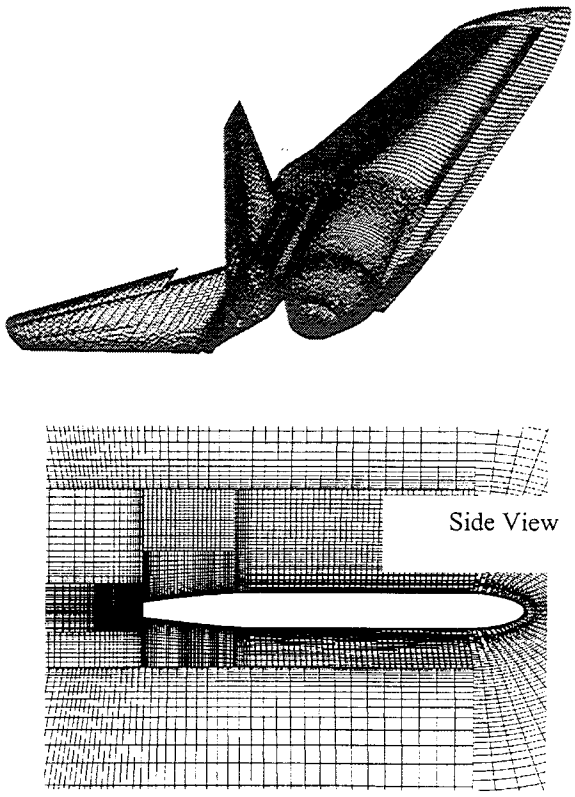

Figure 2a. Mesh for F-15-Like Empenage

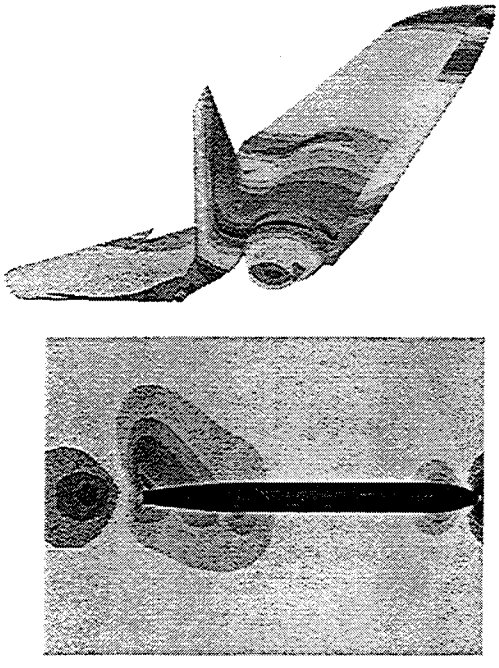

Figure 2b. Pressure Distribution from Rigid Flow Solution

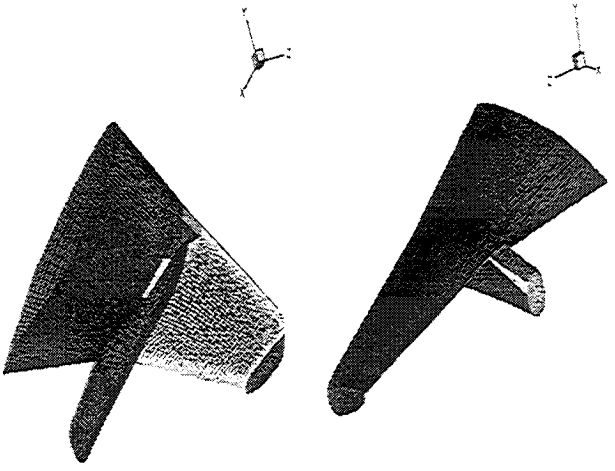

Figure 3. Surface Grid for an AV-8B Wind Tunnel Configuration

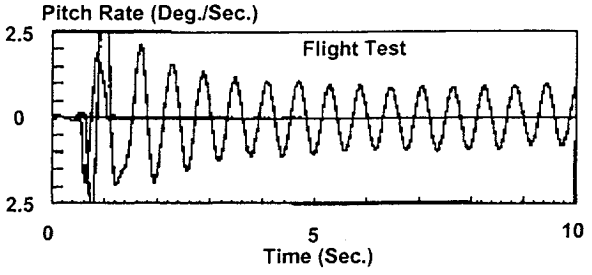

Figure 4. Typical RPO Response to Pitch Doublet

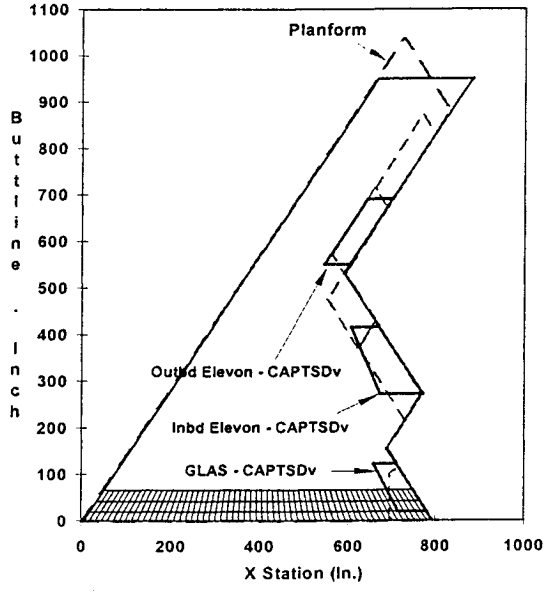

Figure 5. B-2 Planform and CAP-TSDV Aerodynamic Layout

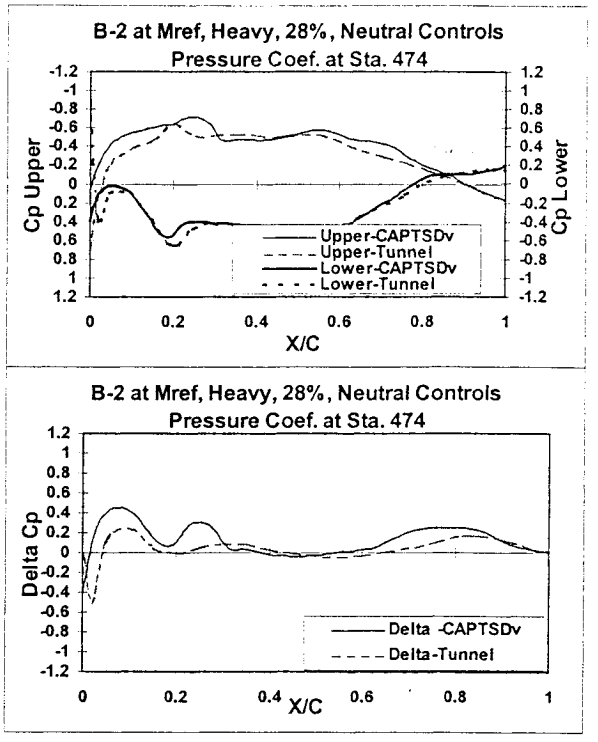

Figure 6. Chordwise Pressure Distribution at Station 474

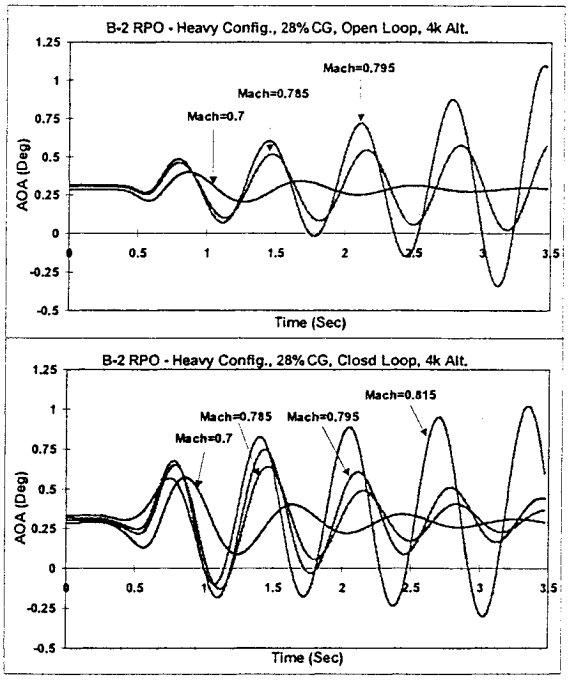

Figure 7. Heavy Configuration AOA Transients (4,000 Alt.)

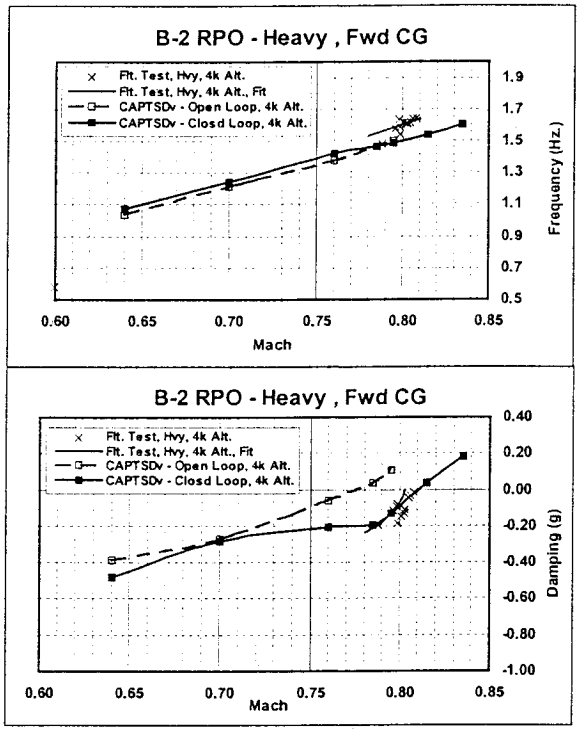

Figure 8. Heavy Configuration Stability Boundary (4,000 Alt.)

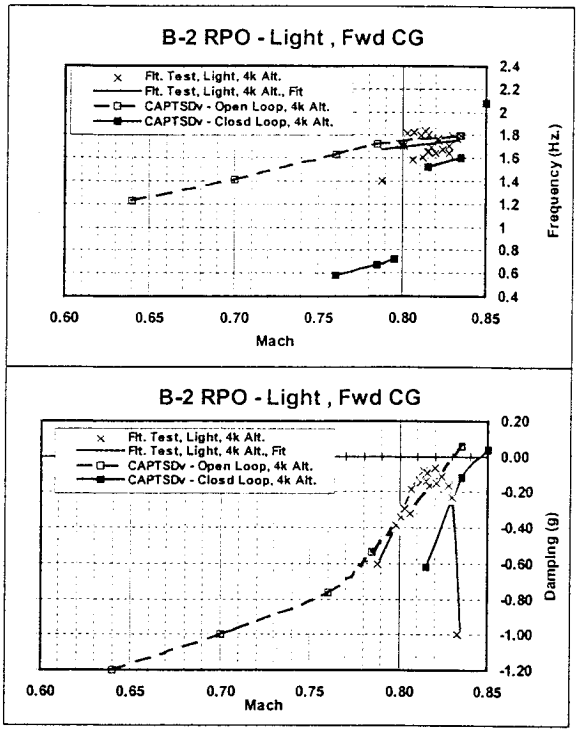

Figure 10. Light Configuration Stability Boundary (4,000 Alt.)

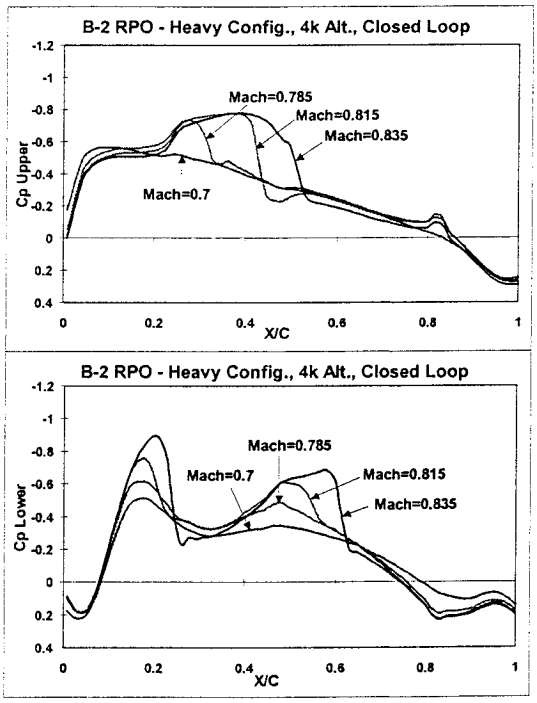

Figure 9. Upper and Lower Surface Pressure Distribution for Various Mach (Station 345)

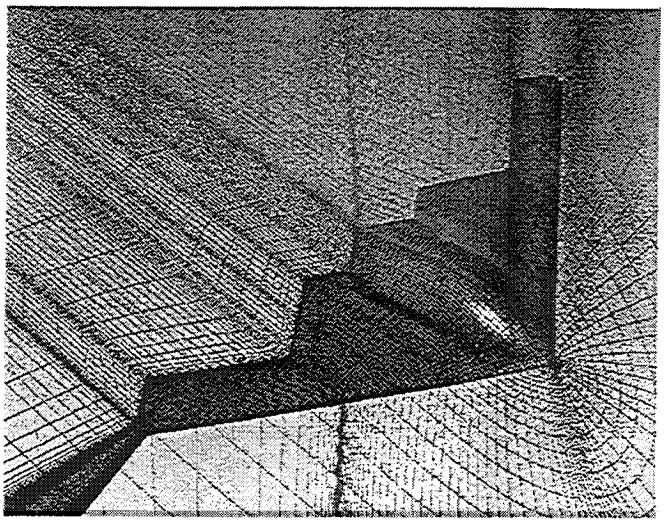

Figure 11. CFL3DAE Navier-Stokes Grid for Aeroelastic Analysis

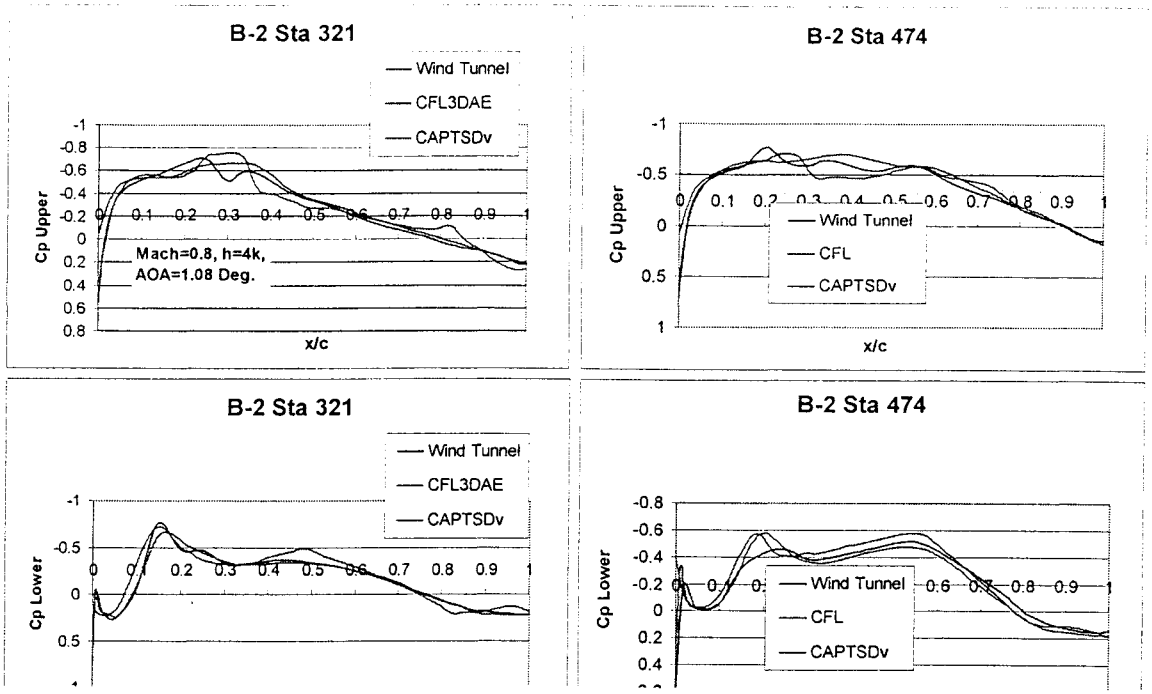

Figure 12. Pressure Distribution - CFL3DAE, Wind Tunnel, and CAP-TSDV

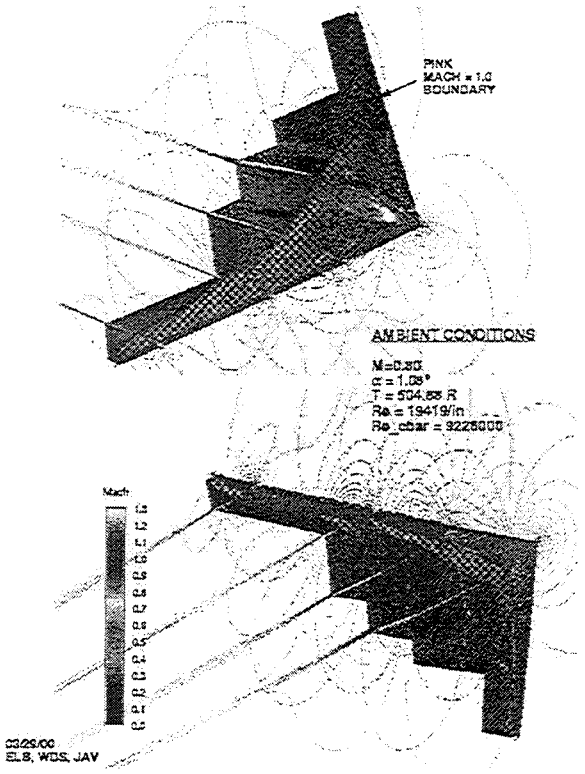

Figure 13. B-2 Mach 1.0 Isosurfaces Near RPO Onset

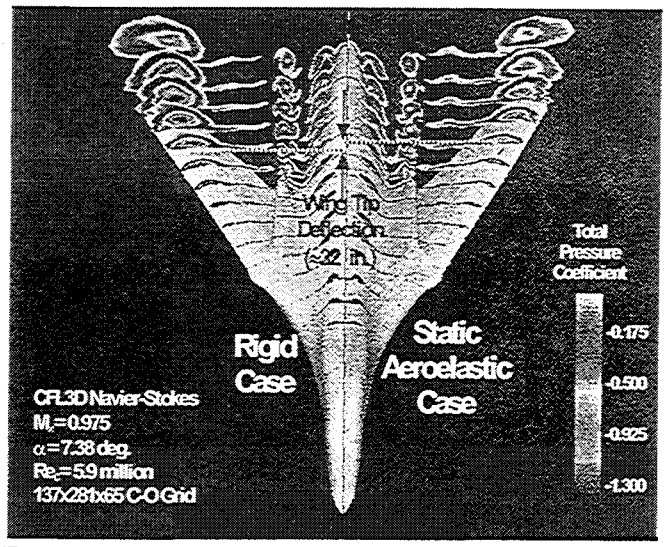

Figure 14. Computed Vortical Flow over a B-1-Like Configuration

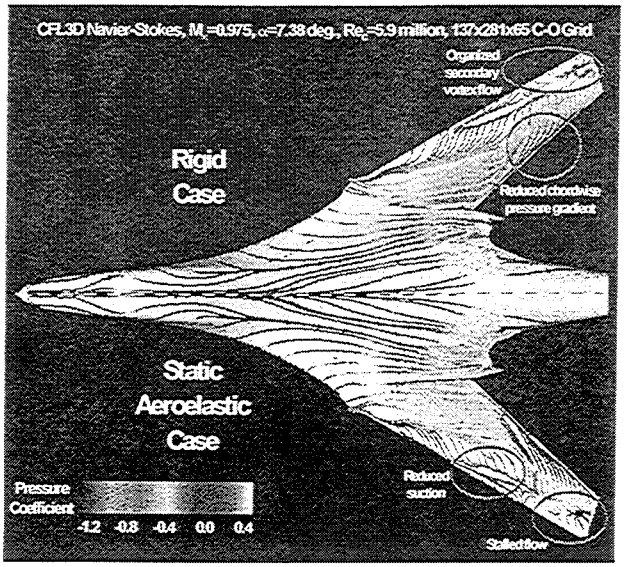

Figure 15. Computed Surface Flow over a B-1-Like Configuration

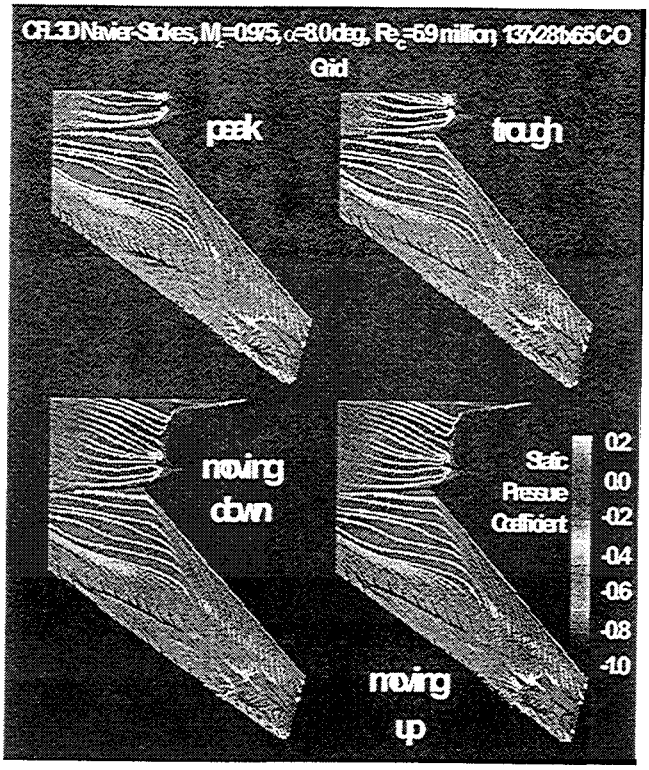

Figure 17. Computed Instantaneous Streamlines for B-1 Wing Undergoing LCO-Like Motion

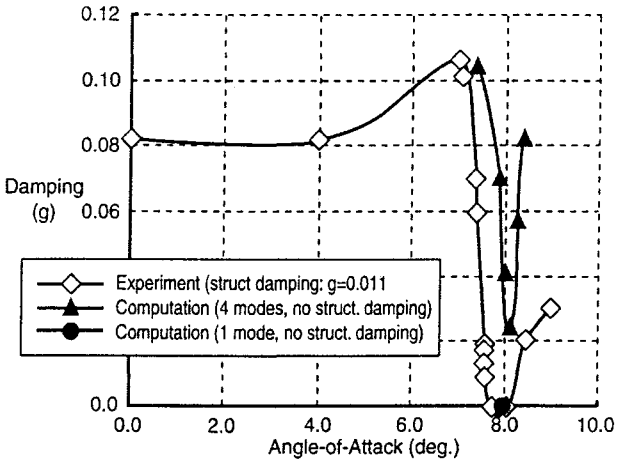

Figure 16. Measured and Computed LCO Damping

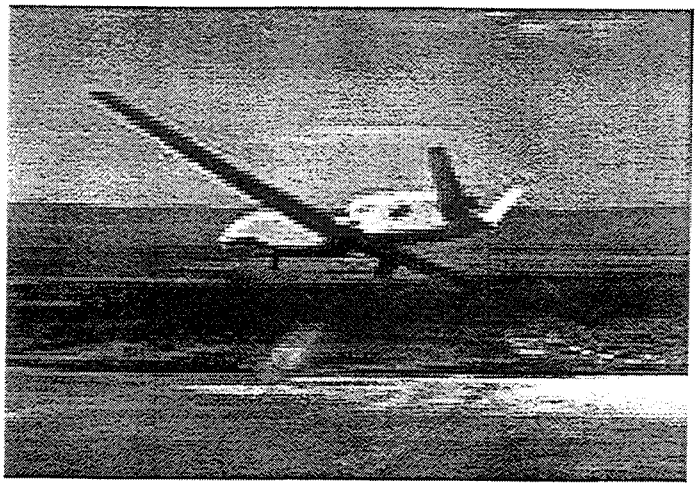

Figure 18. Northrop Grumman Global Hawk

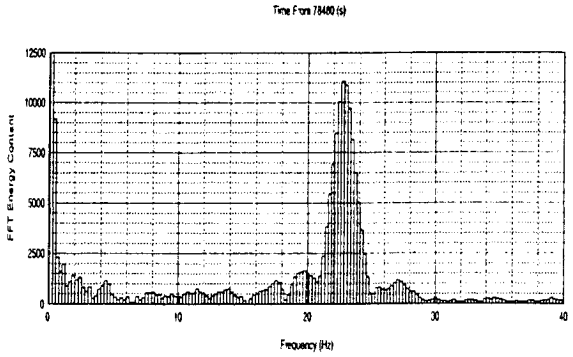

Figure 19. Frequency Domain Plot of Aileron Buzz

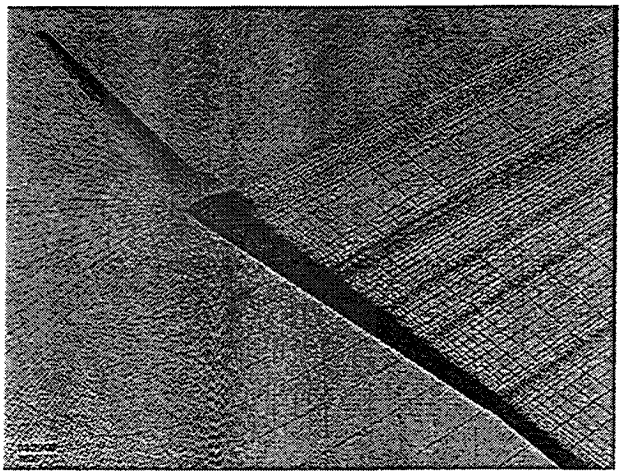

Figure 20. Global Hawk CFD Mesh

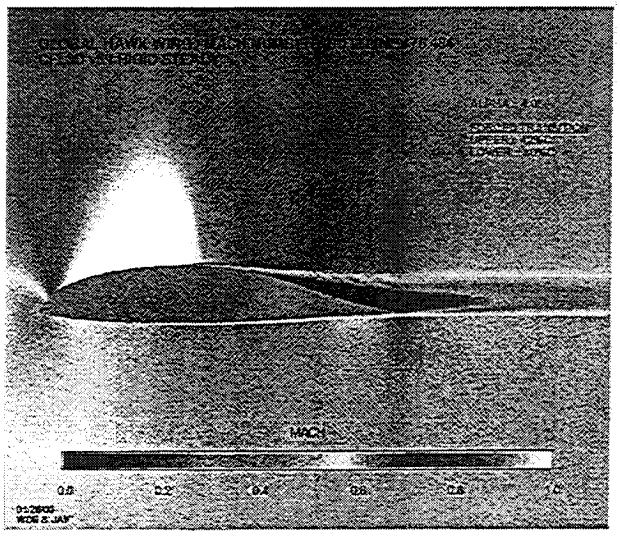

Figure 21. Mach Contours for a Global Hawk Wing Section at Buzz Condition

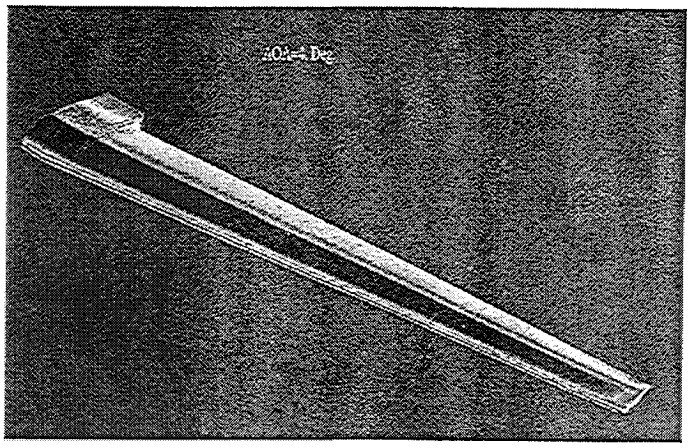

Figure 22. Global Hawk 3D Pressure Contours at Buzz Condition

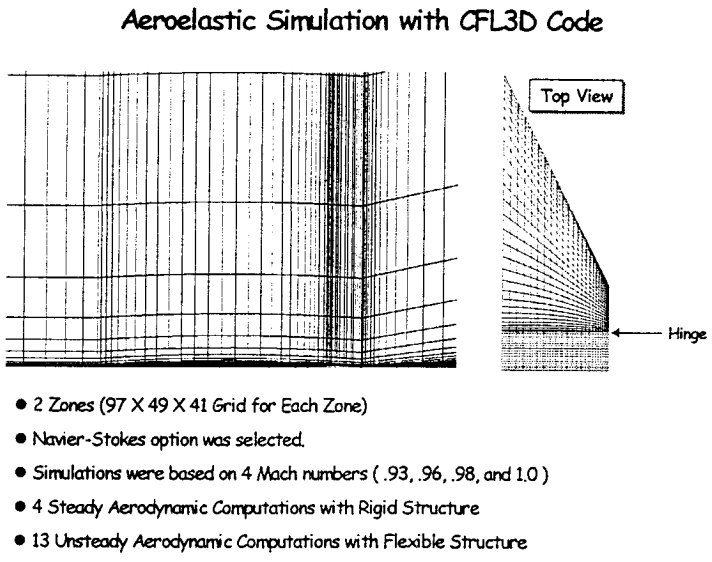

Figure 23. CFL3DAE Grid and Flow Conditions for the Buzz Correlation

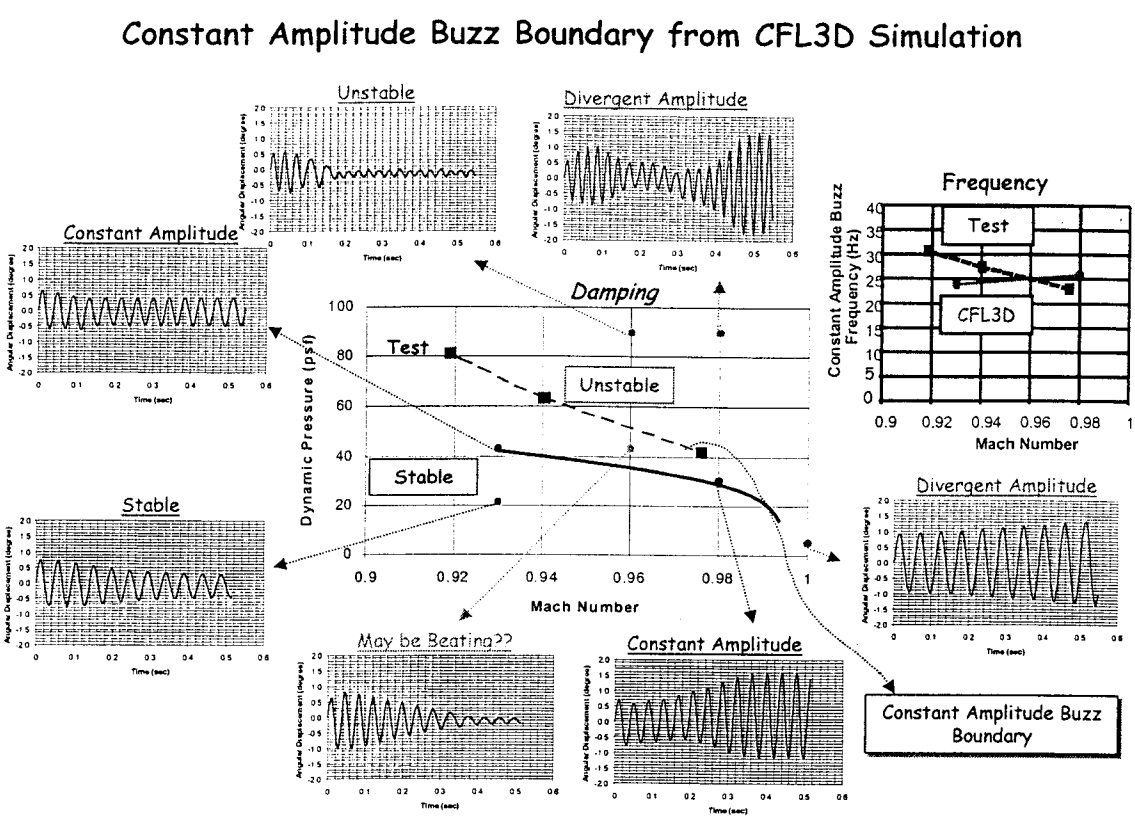

Figure 24. CFL3DAE Damping and Frequency Correlation with Test Data

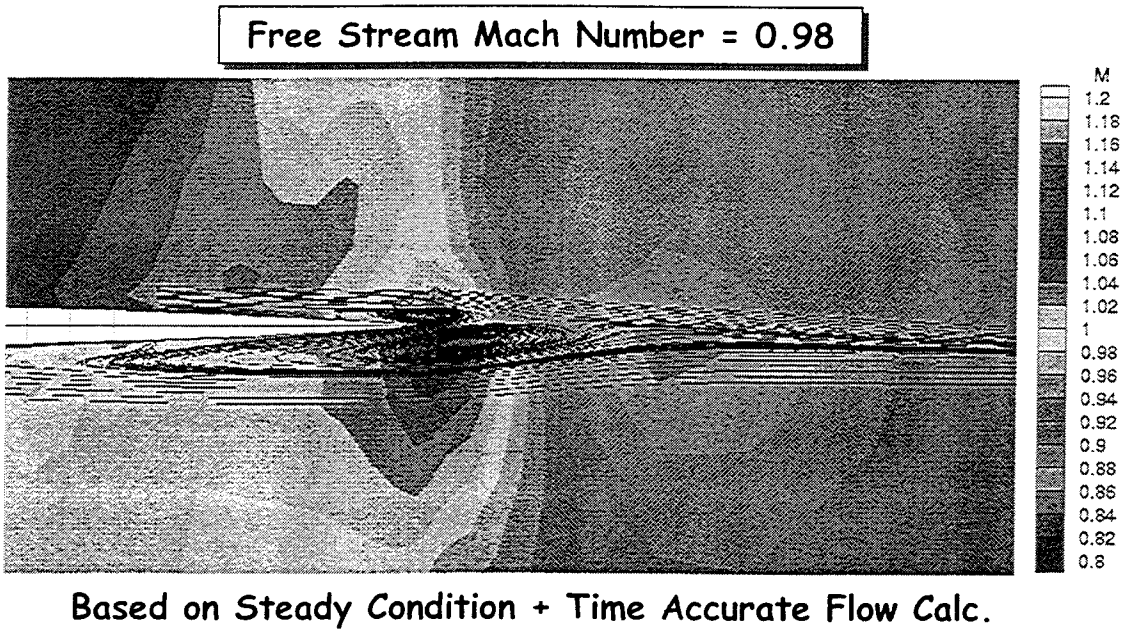

Figure 25. Unsteady Vortex Formation for a Steady Case with CFL3DAE

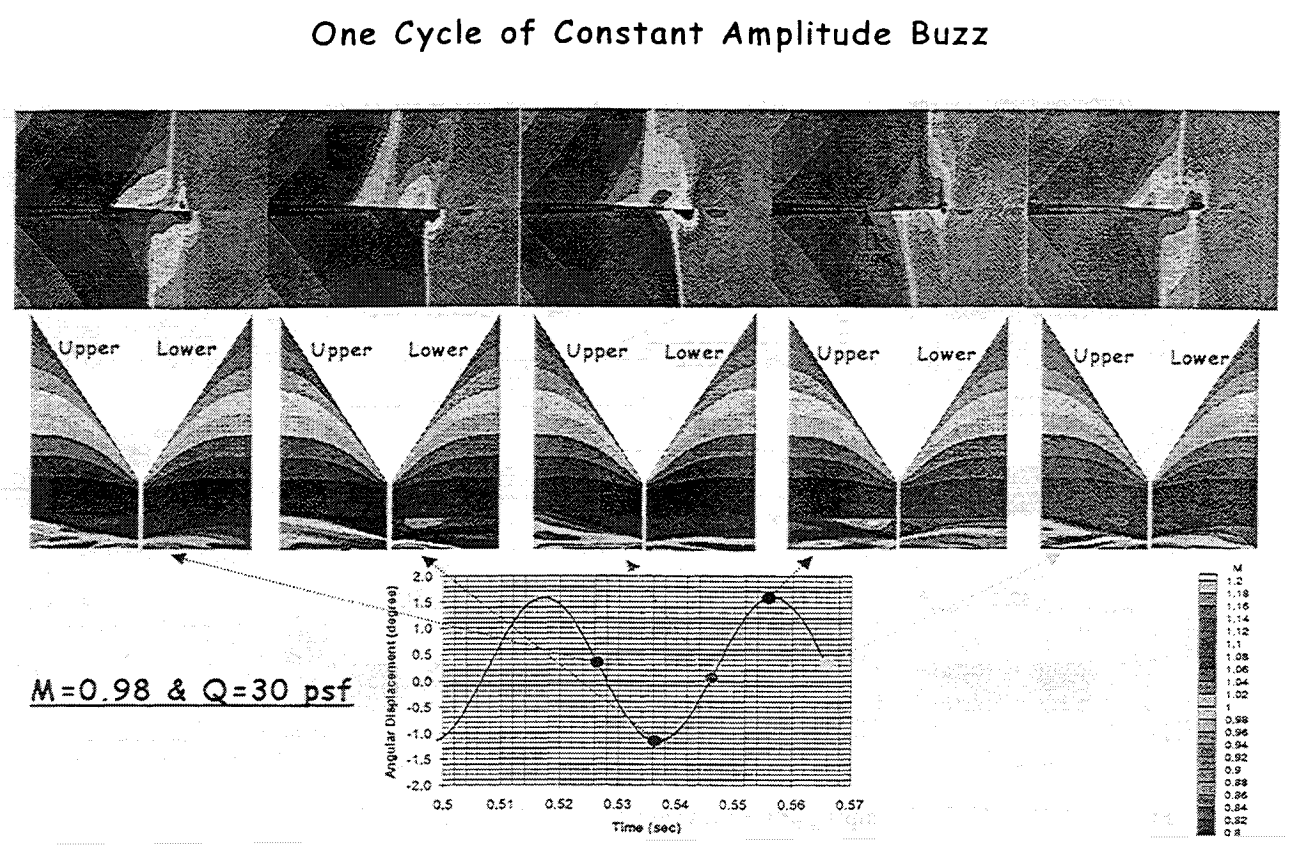

Figure 26. Mach Number Contours for Time Dependent Control Surface Motion

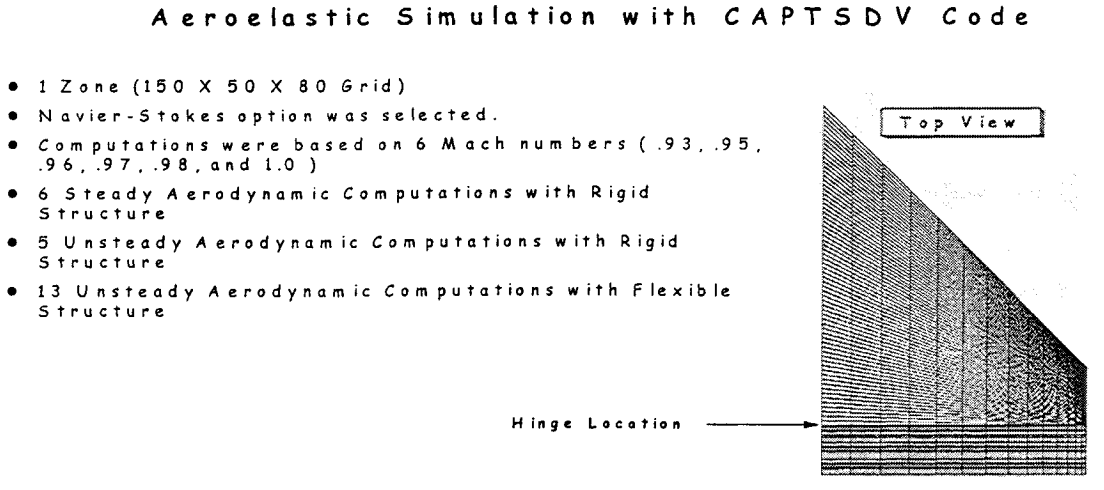

Figure 27, CAP-TSDV Grid and Flow Conditions for the NASP Buzz Correlation

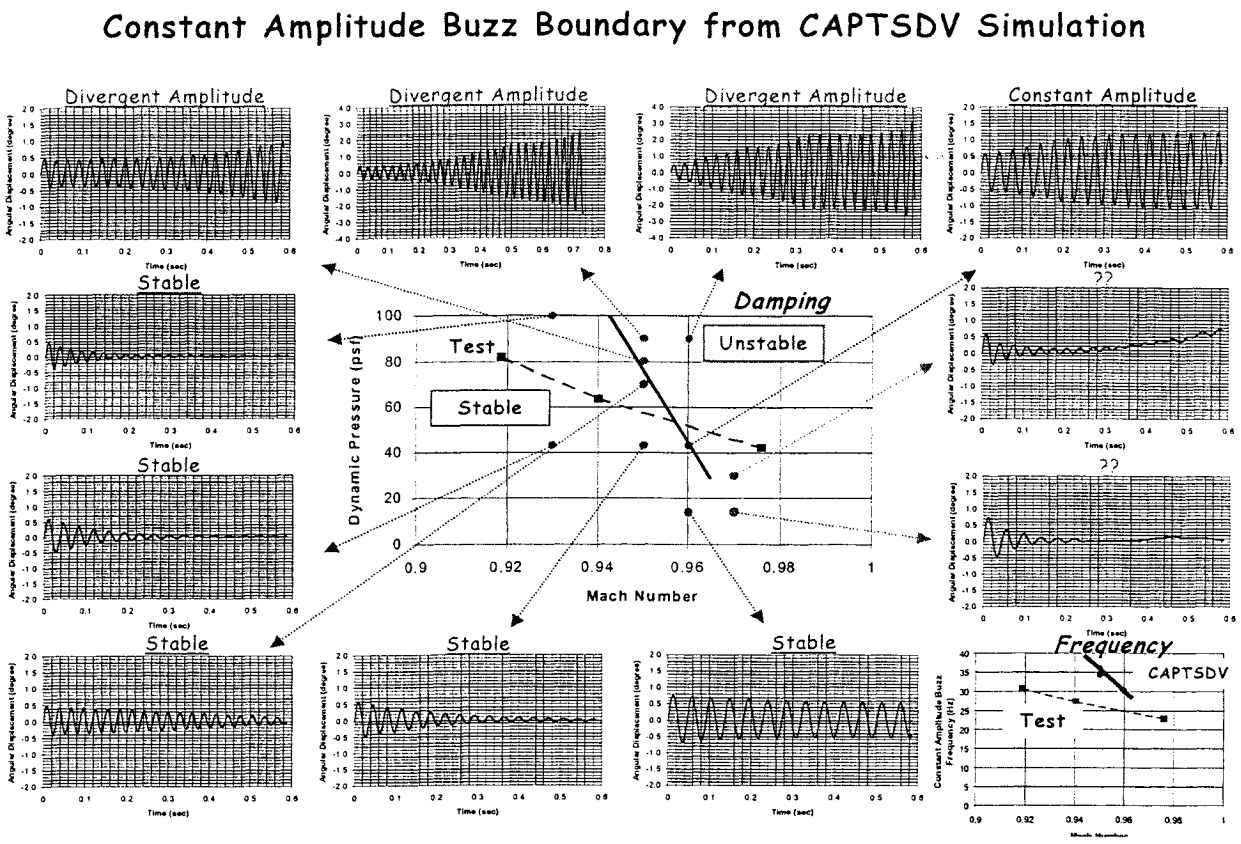

Figure 28. CAP-TSDV Damping and Frequency Correlation with Test Data

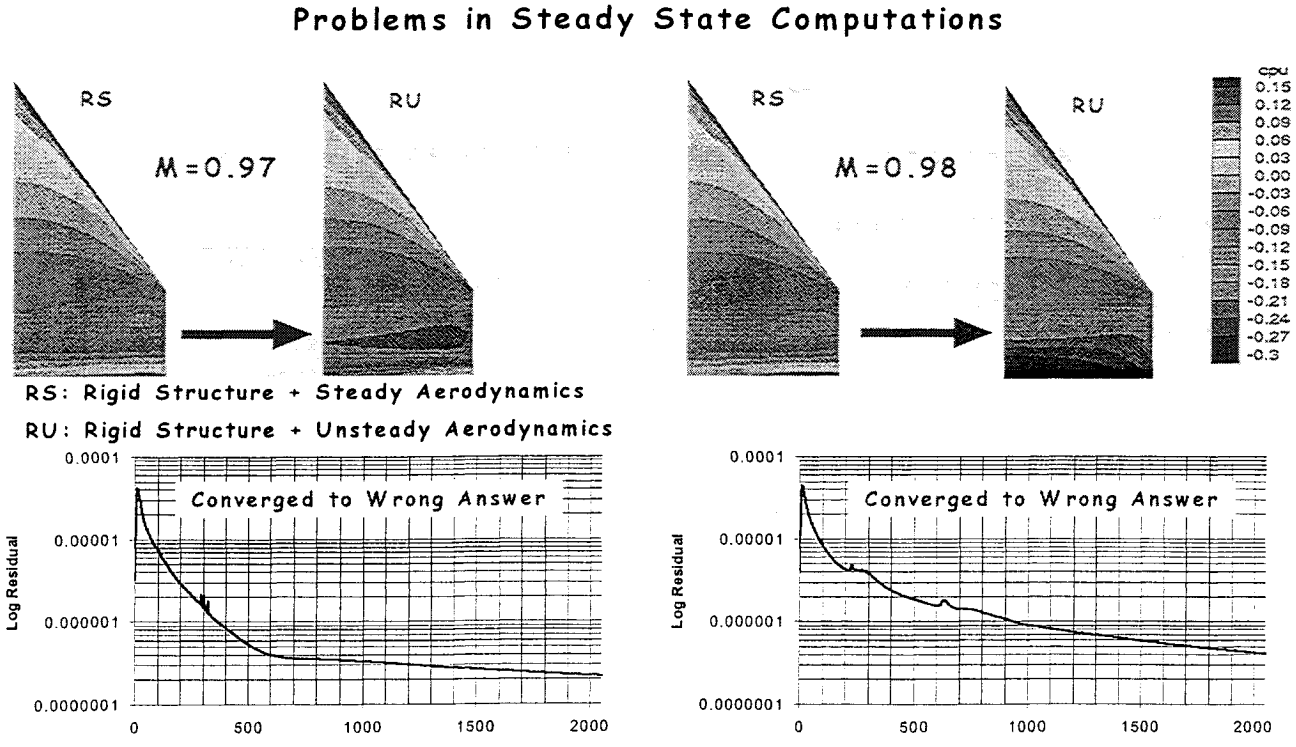

Figure 29. Inconsistency Between Steady and Unsteady Solutions for a Steady Flow